

Modelling damped seismic waves by coupling the Finite Element Method and the Fast Multipole Boundary Element Method

E. Grasso & J.F. Semblat

Université Paris-Est, IFSTTAR, Dept of Geotechnical Eng., Environment and Risks, Paris

S. Chaillat & M. Bonnet

POems (UMR7231 CNRS-ENSTA-INRIA), UMA ENSTA, Paris, France



SUMMARY:

Modelling seismic wave propagation in unbounded media requires sophisticated numerical methods. The Boundary Element method (BEM) is very effective since it accounts implicitly for the radiation conditions at infinity. The fast multipole BEM (FM-BEM) used herein strongly reduces the computational complexity and the memory requirement typical of the classical BEM formulation. This work proposes to couple the FM-BEM and the FEM to take advantage of the versatility of the FEM to model complex geometries and non-linearities and of the exact account for infinite domains, mobile boundaries or unknown boundaries offered by the boundary integral approach. The main idea is to separate one or more bounded subdomains containing complex structures or strong heterogeneities (solved by the FEM) from the complementary semi-infinite viscoelastic space of propagation (solved by the FM-BEM) through a non-overlapping domain decomposition. Two strategies (sequential and simultaneous coupling) have been implemented and their performances compared on simple examples.

Keywords: wave propagation, site effects, numerical modelling, FEM, BEM

1. INTRODUCTION

The coupling of the finite element method (FEM) with the boundary element method (BEM) takes advantage of the versatility of the FEM to model complex geometries and non-linearities and the exact account for infinite domains, mobile boundaries or unknown boundaries offered by the boundary integral approach. Usually, this coupling is realized through conventional approaches or in the framework of the domain decomposition methods. The main idea is to separate the one or more bounded regions containing the vibrating complex structure, any steady source or complex-shaped receiver from the complementary semi-infinite space of propagation. The bounded subdomains are modelled by the FEM, whereas the half-space where they are embedded is solved within the BEM, whose formulation allows the exact physical radiation of the waves in the surrounding soil.

In the present work, interest is focused on wave propagation problems in semi-infinite domains. The fast multipole BEM (FM-BEM) is considered since it strongly reduces the computational complexity and the memory requirement typical of the classical BEM formulation. The media are supposed to have linear viscoelastic behavior. Non-linearities are not considered here, although their treatment may be considered as a natural extension of this work. Various applications of the FEM/BEM coupling may be considered in the field of seismic wave propagation, vibrations in urban environment and dynamic soil-structure interaction (SSI).

After this introductory Section, the paper is organised as follows. In Section 2, the domain decomposition and the resulting interface problem are defined. In Section 3, the main features of the fast-multipole boundary element method (FMBEM) are briefly recalled. Section 4 and 5 are then devoted to the iterative and the simultaneous coupling respectively.

2. DOMAIN DECOMPOSITION AND INTERFACE PROBLEM

2.1 Interface problem statement

Let Ω denote a region of space occupied by a three-dimensional isotropic homogeneous (visco)elastic solid with boundary $\partial\Omega$, as depicted in Fig.2.1(left). Body forces and boundary conditions are assumed time-harmonic with circular frequency ω , the implicit factor $e^{-i\omega t}$ being systematically omitted in the following. As the domain Ω may feature complex geometrical details, heterogeneous or anisotropic materials (all of these features being here assumed to be confined in a bounded region) a solution of the wave propagation problem by pure FM-BEM is not feasible for many applications.

Therefore, a spatial decomposition of Ω into a bounded subdomain Ω_F (which embraces the above mentioned "irregularities") and into its unbounded complement Ω_B (which allows the wave radiation and dispersion at infinity) is introduced, as shown in Fig.2.1 (right). Allowing more flexibility, the finite element method is used to discretize the problem in Ω_F , while the boundary element method is used for the subdomain Ω_B . Possible piecewise homogeneous regions in Ω_B are treated via an internal BE-BE coupling (Chaillat, 2009). The two subdomains Ω_B, Ω_F are supposed to be non-overlapping. The portion of boundary shared by the subdomains is the interface $\Phi = \partial\Omega_B \cap \partial\Omega_F$ (notation Φ_{ij} indicates the portion of surface of the subdomain Ω_i adjacent to Ω_j and having the normal \mathbf{n} oriented from Ω_i to Ω_j).

Continuity of the displacement field and equilibrium of the traction field across the common interface Φ must be enforced through appropriate transmission conditions. In this work, transmission conditions are enforced in a strong sense. Strong coupling conditions require conforming connection of the interface meshes, i.e. that (i) there is a one-to-one correspondence between degrees of freedom on the interface (i.e. meshes coincide) and that (ii) the traces of interpolation functions on the shared faces are the same. In this case, continuity and equilibrium conditions are directly imposed on the interface nodes. The system of local equations governing the elastodynamic problem restricted to each subdomain Ω_s ($s=B,F$) reads (neglecting body forces):

$$\begin{aligned} \nabla \cdot \boldsymbol{\sigma}_s(\mathbf{x}) + \rho_s \omega^2(\mathbf{x}) \mathbf{u}_s(\mathbf{x}) &= 0 \\ \boldsymbol{\varepsilon}_s(\mathbf{x}) &= \frac{1}{2} \left(\nabla \mathbf{u}_s + \nabla \mathbf{u}_s^T \right) (\mathbf{x}) = 0 \\ \boldsymbol{\sigma}_s(\mathbf{x}) &= \mathbf{D}_s : \boldsymbol{\varepsilon}_s(\mathbf{x}) = 0 \end{aligned} \quad (2.1)$$

where ρ_s is the mass density of the domain Ω_s and \mathbf{D}_s is the fourth-order tensor expressing the constitutive behavior. In elasticity, \mathbf{D}_s would be the fourth-order elasticity tensor, whereas in visco-elasticity it would be the relaxation tensor. The boundary conditions of Dirichlet or Neumann type read:

$$\begin{aligned} \mathbf{u}_s(\mathbf{x}) &= \mathbf{u}_s^D(\mathbf{x}) & (\mathbf{x} \in \partial_U \Omega_s) \\ \boldsymbol{\sigma}_s(\mathbf{x}) \mathbf{n}_s(\mathbf{x}) &= \mathbf{t}_s^D(\mathbf{x}) & (\mathbf{x} \in \partial_T \Omega_s) \end{aligned} \quad (2.2)$$

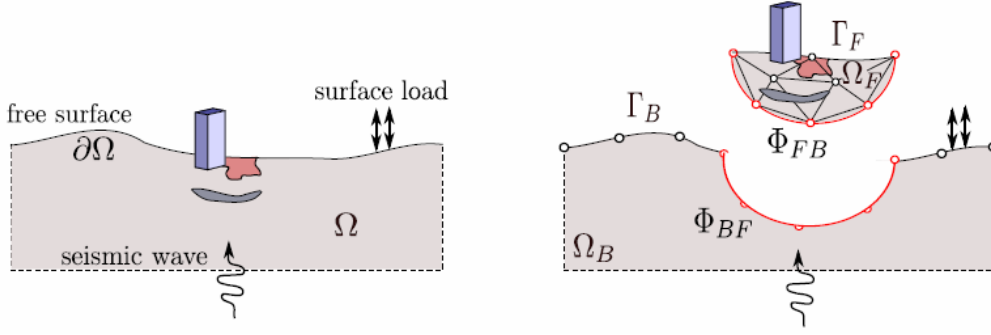


Figure 2.1. Spatial domain decomposition for FEM/BEM coupling: original time-harmonic problem defined in the semi-infinite domain (left) and decomposition in the two non-overlapping subdomains B, discretized by BEM, and F, discretized by FEM (right).

Considering the unit normal \mathbf{n} as pointing outward from each Ω_s , the transmission conditions on each general Φ_{il} read:

$$\begin{aligned} \mathbf{u}^i(\mathbf{x}) &= \mathbf{u}^l(\mathbf{x}) & (\mathbf{x} \in \Phi_{il}) \\ \sigma^i(\mathbf{x}) \cdot \mathbf{n}^i(\mathbf{x}) + \sigma^l(\mathbf{x}) \cdot \mathbf{n}^l(\mathbf{x}) &= 0 & (\mathbf{x} \in \Phi_{il}) \end{aligned} \quad (2.3)$$

2.2 Discretization of the subdomains

The surface of Ω_B is discretized with three-noded triangular boundary elements, and the FE volumes Ω_F are discretized with four-noded isoparametric linear tetrahedral elements. The set of three-noded triangular faces of the tetrahedra lying on the interface Φ constitutes the discretization of the corresponding BEM surface. Consequently, each part of the BEM mesh intersecting the interface Φ and the trace of the FEM three-dimensional mesh on Φ are the same by construction. Moreover, they are associated with the same interpolation functions, namely piecewise linear interpolation of displacements. As the interpolation on the interface is conforming, perfect bonding conditions are expressed in strong form on the nodal values. The two subdomains cannot be solved independently, and the original problem is recovered by the transmission conditions on the interfaces.

3. FAST MULTIPOLE BOUNDARY ELEMENT METHOD

3.1 Boundary element method

The subdomain Ω_B is solved with the boundary element method (BEM) accelerated by the fast multipole method. In the BEM, only the boundary $\partial\Omega_B$ of Ω_B , defined as $\partial\Omega_B = \Gamma_B \cup \Phi_{BF}$ is discretized. For a Neumann problem, the traction DoFs are known on Γ_B and unknown on the interface Φ_{BF} , whereas displacement DoFs are unknown on the whole $\partial\Omega_B$. For $\mathbf{x} \in \partial\Omega_B$, the boundary integral equation (BIE) reads:

$$c_{ik}(\mathbf{x})u_i(\mathbf{x}) + (\text{P.V.}) \int_{\partial\Omega_B} u_i(\mathbf{y})T_i^k(\mathbf{x}, \mathbf{y}; \omega) dS_y - \int_{\partial\Omega_B} t_i(\mathbf{y})U_i^k(\mathbf{x}, \mathbf{y}; \omega) dS_y = 0 \quad (3.4)$$

where $U_i^k(\mathbf{x}, \mathbf{y}; \omega)$ and $T_i^k(\mathbf{x}, \mathbf{y}; \omega)$ are the visco-elastodynamic fundamental solution. After the boundary element discretization of $\partial\Omega_B$, the following linear system of equations rises:

$$H_B U_B - G_B T_B = 0 \quad (3.5)$$

where H_B and G_B are fully populated, non-symmetric integral operators, and U_B, T_B gather all the displacement and traction degrees of freedom.

3.2 Fast multipole method

In the field of physics (Maxwell or Laplace equations), recent advances in boundary element methods lead to a very important decrease of the computational cost. Instead of point to point interaction as in classical boundary element methods, the fast multipole method (Darve, 2000, Greengard et al., 1998, Fujiwara, 2000) considers interactions between groups of points (cells centered on a multipole, Fig. 3.1) and hence avoids multiple computations of nearly identical terms corresponding to very close points.

It is possible to apply this method at a single scale or even at various scales through a multilevel approach. The size of each cell around its multipole depends on the distance to the other cells: the larger the distance between cells, the larger the cells (Fig. 3.1). The computations of the singular integrals are then performed through this approach. They are split in an integral on the surface around the singularity and another integral on the complementary distant surface. The first one is estimated using classical regularization techniques, whereas the latter is computed with a fast multipole algorithm (Greengard et al., 1998). The advantage for the computational cost is very significant since it depends on N^2 for classical methods and on N or $M \log N$ for the fast multipole method (Bonnet et al., 2009, Chaillat et al., 2008). Furthermore, the computational cost is reduced for both the memory storage and the calculation time. This method allows the analysis of very large problems involving millions of unknowns on a single-processor PC (to compare to several tens of thousands previously). Current researches also investigate a fast multipole method well-adapted to the Helmholtz equation and even to elastodynamics (Fujiwara, 2000, Chaillat et al., 2008, 2009). The fast multipole method then allows the computation of very large models considering a larger number of heterogeneities, a more realistic geometrical representation of geological structures (especially in 3D) as well as higher frequency values (detailed modelling of short wavelengths amplification).

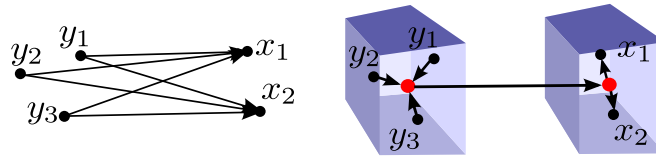


Figure 3.1. Comparison of the principles of the standard BEM (left) and the Fast Multipole BEM (right).

4. ITERATIVE FEM/FMBEM COUPLING

4.1 Proposed algorithm

To solve the coupled problem we use a single relaxation sequential Dirichlet-Neumann algorithm. This is a modified version of the algorithm proposed by Lin for linear elastostatics (Lin, 1996) and consists in an interface relaxation algorithm.

First, the FM-BEM is used to pre-compute the scattered displacement field $\mathbf{u}_{B_S}(\mathbf{x})$ induced on the boundary $\Gamma_B \cup \Phi_{BF}$ of Ω_B (where $\Gamma_B = \Omega_B \cap \partial\Omega$) by the incident wave. The corresponding solution in terms of total field is obtained by adding the incident wave field to the scattered solution, i.e. $\mathbf{u}_B(\mathbf{x}) = \mathbf{u}_{B_S}(\mathbf{x}) + \mathbf{u}_{B_I}(\mathbf{x})$. Then, after invoking continuity conditions, the restriction \mathbf{u}_B^Φ of \mathbf{u}_B to the interface Φ_{BF} is relaxed and employed as initial guess for the iterative algorithm. At this point, the solution of the global problem involves the alternating resolution of a local Dirichlet problem in the FE subdomain and of a local Neumann problem in the BE subdomain until convergence of the

displacement field on Φ is reached. At a given iteration n , the former implies the resolution of the FEM system for \mathbf{u}_F , followed by the computation of total interface tractions $\mathbf{t}_{F,n}^\Phi$. The scattered traction field, $\mathbf{t}_{F_S,n}^\Phi = \mathbf{t}_{F,n}^\Phi - \mathbf{t}_{F_I,n}^\Phi$, is then applied to the BE-interface Φ_{BF} after invoking continuity $\mathbf{t}_{B,n}^\Phi = -\mathbf{t}_{F_S,n}^\Phi$.

4.2 Example of far field excitation: scattering by a semi-spherical canyon

To assess the iterative algorithm for far field excitations sources, the canonical problem of the scattering of a vertically incident P-wave on unit amplitude has been considered. The medium is assumed to be constituted by a single material, characterized by normalized values of the shear modulus $\mu=2$, Poisson's ratio $\nu=0.25$ and density $\rho=2$. To assess the accuracy of the solution, the surface displacements field computed on the coupled problem with the sequential iterative algorithm has been compared to the corresponding solution computed by using only the FM-BEM method.

Results obtained with this iterative coupling approach are quite satisfactory, as shown in Fig. 4.1, where the absolute vertical displacement on the positive x-axis is reported for two values of damping ratio $\beta=0$ (top), 0.05 (bottom) at normalized frequencies $\eta_P=0.25$ (a,c) and $\eta_P=0.5$ (b,d). However, the range of the relaxation parameter to obtain convergence has been established for each treated problem, and no empirical parametric studies have been conducted to extrapolate global range of validity.

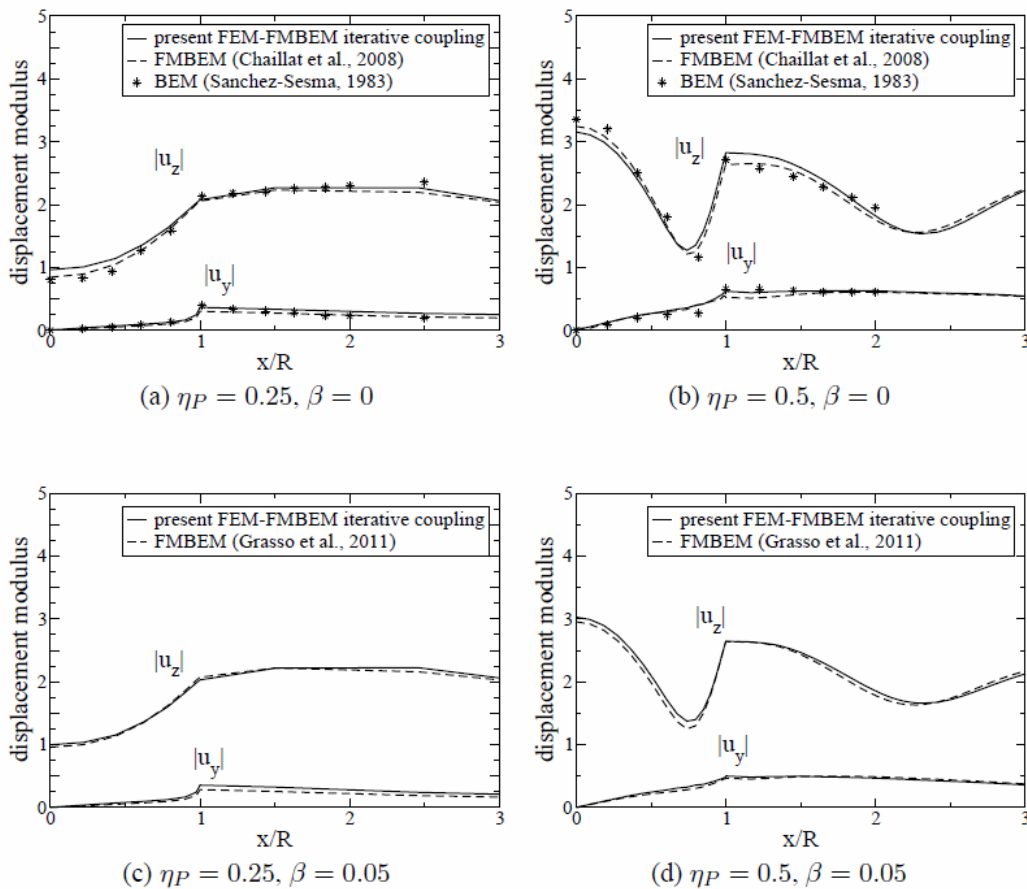


Figure 4.1. Scattering of a vertically incident P-wave by a semi-spherical canyon at normalized frequency: surface displacements $|u_y|$ and $|u_z|$ for two values of damping ratio $\beta=0$ (top) and 0.05 (bottom) at normalized frequencies $\eta_P=0.25$ (left) and $\eta_P=0.5$ (right).

4.3 Refinement of the iterative algorithm

The iterative interface relaxation algorithms proposed above have two main drawbacks. The first is that the convergence depends on the chosen value of the relaxation parameter θ . The second consists in the fact that each global iteration a priori requires N_{FMBEM} internal GMRES iterations for the fast solution of the BE global system, i.e. $N_{\text{glob}} \times N_{\text{FMBEM}}$ iterations are needed for a complete computation. This disadvantage can be reduced by setting at each new global iterate the GMRES initial guess to the solution of the previous iterate. This modification is simple to implement and has a strong influence on the acceleration of the convergence process. This is shown for a simple example test in Fig. 4.2 where the dotted line indicates the convergence acceleration induced by this refinement of the algorithm.

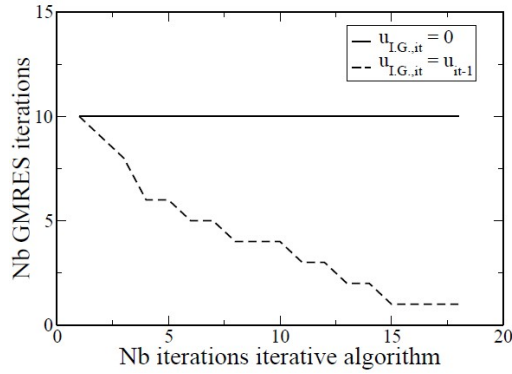


Figure 4.2. Number of iterations of GMRES solver when setting the Initial Guess (I.G.) to zero $u_{I.G.,it}=0$ or to the solution at the previous iteration $u_{I.G.,it}=u_{it-1}$. Results in (a) and (b) refer to the scattering of a vertically incident P-wave by a semi-spherical canyon test.

5. SIMULTANEOUS FEM/FMBEM COUPLING

5.1 Proposed algorithm

The second strategy that we present for coupling the FEM and the FMBEM is a simultaneous approach based on solving a global system of equations combined with the transmission conditions across the common interface. In particular, we apply a modified version of the approach proposed in (Frangi,2006) based on an implicit condensation for the FEM degrees of freedom. The global system is then solved by generalized minimal residual (GMRES).

After separation of internal and interface degrees of freedom, the FEM displacement-based linear system reads:

$$\begin{bmatrix} \mathbf{K}_F^F & \mathbf{K}_{FB}^F \\ \mathbf{K}_F^{FB} & \mathbf{K}_{FB}^{FB} \end{bmatrix} \begin{Bmatrix} \mathbf{u}_F \\ \mathbf{u}_{FB} \end{Bmatrix} = \begin{Bmatrix} 0 \\ \mathbf{f}_{FB} \end{Bmatrix} \quad (5.6)$$

For a surface loading, the BEM linear system can be written:

$$H_B U_B - G_B T_B = 0 \quad (5.7)$$

where separation of unknowns leads to

$$\begin{bmatrix} \mathbf{H}_B^B & \mathbf{H}_{BF}^B & -\mathbf{G}_{BF}^B \\ \mathbf{H}_B^{BF} & \mathbf{H}_{BF}^{BF} & -\mathbf{G}_{BF}^{BF} \\ \overline{\mathbf{H}}_B^B & \overline{\mathbf{H}}_{BF}^B & -\overline{\mathbf{G}}_{BF}^B \\ \overline{\mathbf{H}}_B^{BF} & \overline{\mathbf{H}}_{BF}^{BF} & -\overline{\mathbf{G}}_{BF}^{BF} \end{bmatrix} \begin{Bmatrix} \mathbf{u}_B \\ \mathbf{u}_{BF} \\ \mathbf{t}_{BF} \end{Bmatrix} = \begin{bmatrix} \mathbf{b}_B^B \\ \mathbf{b}_B^{BF} \\ \overline{\mathbf{b}}_B^B \\ \overline{\mathbf{b}}_B^{BF} \end{bmatrix} \quad (5.8)$$

In the simultaneous approach, the FEM system is solved implicitly in the FMBEM system. The displacements on the FE-BE interface Φ are chosen as primary unknowns, and continuity across the interface Φ is guaranteed by the strong condition. The Algorithm is detailed hereafter.

Algorithm 3 Simultaneous coupling algorithm

- 1: **Pre-step** Domain decomposition of Ω in non-overlapping Ω_F and Ω_B (Sec. 3.6.2)
- 2: Discretization of Ω_F (3-D) and $\partial\Omega_B$ (2-D), definition of Φ_{FB} and Φ_{BF}
- 3: Define and store vector of corresponding interface nodes
- 4: Define FEM problem in Ω_F , store coordinates and connectivity tables
- 5: Set up and store sparse \mathcal{K}_F and \mathbb{F}_F (eq.(3.14))
- 6: Define FMBEM problem in Ω_B and prepare data and geometry input file

Main algorithm

- 7: Definition of the FMM-octree for $\partial\Omega_B$
 - 8: Compute and store BEM near contributions \mathbb{K}^{near} and \mathbb{F}^{near} (eq.(2.17b))
 - 9: Read stored FEM- \mathcal{K}_F , $-\mathbb{F}_F$, -coordinates and -connectivity tables
 - 10: Initialize GMRES (solution vector and restart parameter)
 - 11: **for** $n = 0, k$ **do**
 - 12: Compute $\tilde{\mathbb{F}}_F^n$ associated with the approximated displacements $\tilde{\mathbf{u}}_{FB}$
 - 13: Solve FEM system (3.19)
 - 14: Compute $\tilde{\mathbf{t}}_{FB}^n$ and substitute back in $\tilde{\mathbb{X}}_B^n$
 - 15: FMM matrix-vector product and compute residual
 - 16: **if** convergence **then**
 - 17: stop
 - 18: **end if**
 - 19: **end for**
-

5.2 Validation and examples

The simultaneous FEM/FMBEM algorithm has been tested on various 3-D examples, which have been chosen deliberately simple to allow a direct comparison with pure FMBEM results. As depicted in Fig. 5.1, we first consider a time-harmonic surface loading at normalized frequency $\eta_P = k_P R_F / 2\pi = 1$, where R_F is the radius of the FEM subdomain. The plane BE-free surface $\Gamma_B = \Omega_B \cap \partial\Omega$ has been truncated at a distance $R_B = 4R_F$. For simplicity, radius R_F has been chosen of unit length, thus resulting in $R_B = 4$. The circular portion of surface ∂T on which time-harmonic tractions are imposed has radius 0.2 and it is located at a distance $R_t = 2$ from the axis origin. Fig. 5.2 shows the contour plot of the vertical and horizontal displacements in the x-y plane. The little circular solid line centered in the origin is the soft basin, whereas the dotted line is the trace of the interface Φ on the plane free surface. A comparison between the coupled approach and pure FM-BEM computations is also proposed in Fig. 5.3. As shown in the figure, the computed vertical and horizontal displacements are very close.

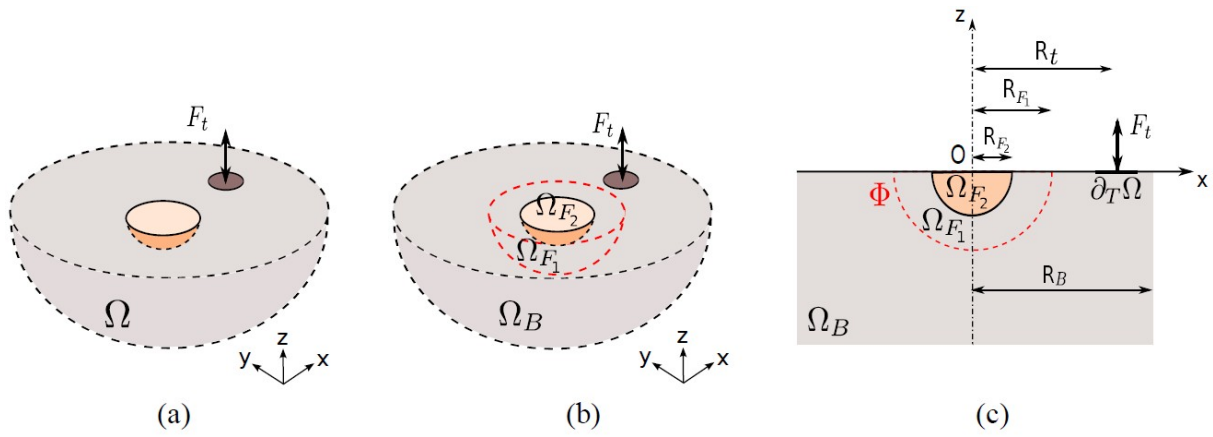


Figure 5.1. Time-harmonic load on a homogeneous half-space containing a soft superficial basin: geometry, domain decomposition and notation.

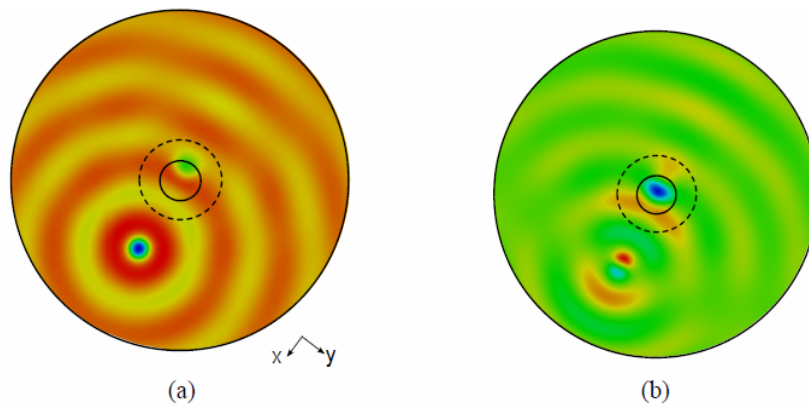


Figure 5.2. Time-harmonic load on a homogeneous half-space containing a soft superficial basin. Contour of the real vertical (a) and horizontal (b) displacements ($\beta=0$, $\eta_p=0.75$).

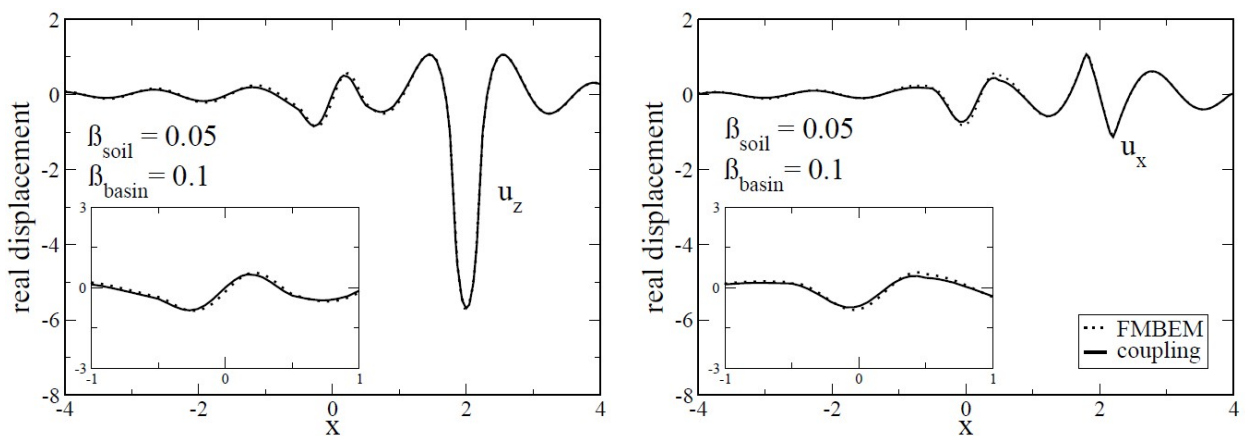


Figure 5.3. Time-harmonic load on a homogeneous half-space containing a soft superficial basin: real vertical u_z and horizontal u_x displacements along the x -axis at normalized frequency $\eta_p = 0.75$. The wavevelocity in the soil worth $c_s(\text{soil}) = 2 c_s(\text{basin})$. Damping factors are $\beta_{\text{soil}} = 0.05$ and $\beta_{\text{basin}} = 0.1$.

5.3 Accuracy and sensitivity

A mesh density study has shown that the numerical results (obtained by using the rule of thumb with 10 points per S-wavelength in the FEM subdomain) are affected by numerical dispersion (Semblat and Brioist, 2000). Using finer FE meshes allows to improve accuracy but at the price of higher computational costs because of over-refinement in stiffer regions (its is aggravated by the assumption of matching grids at the FE-BE interface). A summary of the sensitivity study for various FE mesh refinements is proposed in Fig. 5.5.

The influence of the FE mass matrix formulation on numerical dispersion is also strong. As shown in Fig. 5.4, the comparison with pure FM-BEM computations is better for the lumped FE mass matrix. The results of the sensitivity study for various FE mesh refinements as well as different FE mass matrix formulations is proposed in Fig. 5.5.

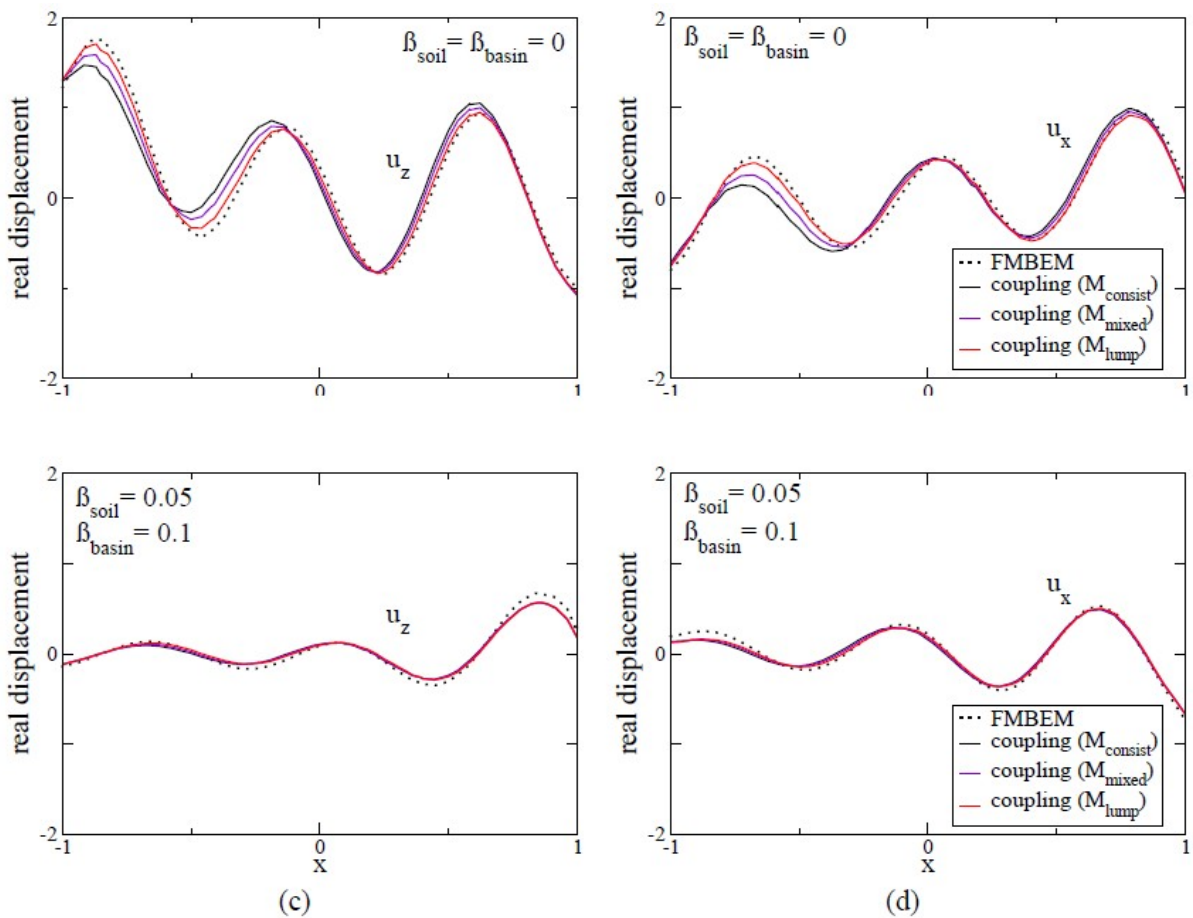


Figure 5.4. Influence of the definition of the FEM mass matrix on simultaneous FEM/FMBEM coupling results for a given test problem. Results show how attenuation strongly reduce the influence of the mass definition (bottom), so clear in the purely elastic case (top).

6. CONCLUSIONS

In this paper, a coupling between the finite element method and the fast-multipole boundary element method is proposed to solve 3D timeharmonic linear elastic problems over unbounded domains. A sequential interface relaxation method (IRM) is first considered. The method is based on a domain decomposition in several disjoint, non-overlapping subdomains. A bounded subdomain is modelled by the finite element method, whereas the half-space where it is embedded is solved by the boundary

element method. At each iteration of the algorithm, a smoothing procedure is applied on the boundary conditions transmitted between the subdomains in order to guarantee and speed up the convergence. This simple algorithm gives interesting results but also deserves further investigations in the near future (e.g. modelling of dynamic soil-structure interaction).

FEM Mass matrix Pts/ λ_S	$M_{consist}$			M_{lump}		
	10	15	20	10	15	20
	$\beta = 0$					
Nb. Iter	18	18	18	19	18	18
CPU/Iter. [sec]	14	58	170	16	59	100
ξ	0.01	0.05	0.046	0.06	0.044	0.042
	$\beta = 0.05$					
Nb. Iter	13	13	14	13	13	13
CPU/Iter. [sec]	20	51	256	23	74	240
ξ	0.051	0.047	0.045	0.039	0.037	0.034
	$\beta = 0.1$					
Nb. Iter	10	11	12	10	10	11
CPU/Iter. [sec]	19	71	310	29	58	247
ξ	0.027	0.025	0.024	0.024	0.023	0.021

Figure 5.5. Time-harmonic load on homogeneous half-space containing a soft inclusion at normalized frequency $\eta_p=1$: comparison between two different formulations for the FEM mass matrix. The GMRES accuracy is here set to $\varepsilon=10^{-2}$ (coupling) and $\varepsilon=10^{-3}$ (FMBEM).

In a next step, a simultaneous approach to couple the finite element method and the fast multipole boundary element method has been proposed to model three-dimensional viscoelastodynamics problems in unbounded domains. The algorithm is based on the fast solution of the BEM global system of equations and by an implicit condensation of the FEM internal degrees of freedom performed at each global GMRES iteration. This approach has been applied on examples having very simple shapes in order to allow an easy comparison with the reference results obtained from pure FM-BEM computations. This algorithm has proved to be stable after the introduction of various forms of heterogeneities, including strong material contrast at the FE/BE interface. Several issues may be considered in the near future to improve the efficiency and interest of the coupling method: non-conforming coupling, material non-linear behaviour, poro-elastodynamics, etc.

REFERENCES

- Bonnet, M. (1999). Boundary integral equation methods for solids and fluids, Wiley, U.K.
- Bonnet, M., Chaillat, S., Semblat, J.F. (2009). Multi-level fast multipole BEM for 3-D elastodynamics, in Recent advances in Boundary Element Methods, Springer.
- Chaillat S., Bonnet M., Semblat J.F. (2008). A multi-level Fast Multipole BEM for 3-D elastodynamics in the frequency domain, *Computer Methods in Applied Mechanics and Eng.*, **197:49-50**, 4233-4249.
- Chaillat S., Bonnet M., Semblat J.F. (2009). A new fast multi-domain BEM to model seismic wave propagation and amplification in 3D geological structures. *Geophysical Journal International*, **177**, 509-531.
- Darve E. (2000). The fast multipole method: Numerical implementation. *J. Comp. Phys.*, **160**, 195-240.
- Frangi A., Ghezzi L. and Faure-Ragani P. (2006). Accurate force evaluation for industrial magnetostatics applications with fast BEM-FEM approaches. *CMES*, 15, n.1:41-48.
- Fujiwara H. (2000). The fast multipole method for solving integral equations of three-dimensional topography and basin problems. *Geophysical Journal International*, **140**, 198-210.
- Greengard L., Huang J., Rokhlin V., and Wandzura S. (1998). Accelerating fast multipole methods for the Helmholtz equation at low frequencies. *IEEE Comp. Sci. Eng.*, **5:3**, 32-38.
- Liu H.-P., Anderson D.L. and Kanamori H. (1976). Velocity dispersion due to anelasticity: Implications for seismology and mantle composition. *Geophysical Journal Royal Astronomical Society*, 47:41-58.
- Semblat J.F., Brioist J.J. (2000). Efficiency of higher order finite elements for the analysis of seismic wave propagation. *Journal of Sound and Vibration*, **231**, 460-467.